NIH Public Access
Author Manuscript
Neurobiol Dis. Author manuscript; available in PMC 2013 May 13.

Published in final edited form as:
Neurobiol Dis. 2006 May ; 22(2): 284–293. doi:10.1016/j.nbd.2005.11.008.

Visual deficits in a mouse model of Batten disease are the result of optic nerve degeneration and loss of dorsal lateral geniculate thalamic neurons

Jill M. Weimer[a], **Andrew W. Custer**[a], **Jared W. Benedict**[a], **Noreen A. Alexander**[d,e], **Evan Kingsley**[a], **Howard J. Federoff**[a,b], **Jonathan D. Cooper**[d,e], and **David A. Pearce**[a,b,c,*]

David A. Pearce: david_pearce@urmc.rochester.edu

[a]Center for Aging and Developmental Biology, University of Rochester School of Medicine and Dentistry, Rochester, NY 14642, USA

[b]Department of Neurology, Aab Insitute of Biomedical Sciences, University of Rochester School of Medicine and Dentistry, Rochester, NY 14642, USA

[c]Department of Biochemistry and Biophysics, University of Rochester School of Medicine and Dentistry, Rochester, NY 14642, USA

[d]Pediatric Storage Disorders Laboratory, MRC Social Genetic and Developmental Psychiatry Centre, Institute of Psychiatry, De Crespigny Park, King's College London, London SE5 8AF, UK

[e]Department of Neuroscience, MRC Social Genetic and Developmental Psychiatry Centre, Institute of Psychiatry, De Crespigny Park, King's College London, London SE5 8AF, UK

Abstract

Juvenile neuronal ceroid lipofuscinosis (JNCL) is an autosomal recessive disorder of childhood caused by mutations in *CLN3.* Although visual deterioration is typically the first clinical sign to manifest in affected children, loss of *Cln3* in a mouse model of JNCL does not recapitulate this retinal deterioration. This suggests that either the loss of *CLN3* does not directly affect retinal cell survival or that nuclei involved in visual processing are affected prior to retinal degeneration. Having previously demonstrated that $Cln3^{-/-}$ mice have decreased optic nerve axonal density, we now demonstrate a decrease in nerve conduction. Examination of retino-recipient regions revealed a decreased number of neurons within the dorsal lateral geniculate nucleus (LGNd). We demonstrate decreased transport of amino acids from the retina to the LGN, suggesting an impediment in communication between the retina and projection nuclei. This study defines a novel path of degeneration within the LGNd, providing a mechanism for causation of JNCL visual deficits.

Keywords

Juvenile neuronal ceroid lipofuscinosis; *CLN3*; Lateral geniculate nucleus; Thalamus; Axonal transport

© 2005 Elsevier Inc. All rights reserved.

*Corresponding author. Center for Aging and Developmental Biology, University of Rochester School of Medicine and Dentistry, Box 645, Rochester, NY 14642, USA. Fax: +1 585 506 1972.

NIH-PA Author Manuscript
NIH-PA Author Manuscript
NIH-PA Author Manuscript

NIH-PA Author Manuscript

NIH-PA Author Manuscript

NIH-PA Author Manuscript

Introduction

Juvenile neuronal ceroid lipofusinosis (JNCL), more commonly known as Batten disease, is a member of a large family of autosomal recessive disorders characterized by the hallmark accumulation of autofluorescent material within lysosomes. The genetic defect associated to Batten disease is a mutation of *CLN3*, a gene which encodes a 438-amino-acid protein of unknown function (Consortium, 1995; Mitchison et al., 1999). The visual system in JNCL patients is affected relatively early in disease progression, with visual deficits typically the first clinical sign to manifest in patients. The onset of this symptom occurs around 4– 7 years of age and culminates in total blindness within several years. The disease progresses to include seizures, motor coordination deficits, memory loss, and typically results in premature death around the third or fourth decade of life (Hofman et al., 1999).

Pathological examination of the retina in JNCL patients at autopsy has revealed a substantial degeneration of photoreceptors, loss of the outer nuclear layer, a reduction in accumulation of lipofuscin granules within the retinal pigmented epithelium (RPE), and accumulation of ceroid, a pathological autofluorescent storage material, within the retinal ganglion cells (RGCs) (Goebel et al., 1974; Bensaoula et al., 2000). Although the disease appears to commence in the peripheral regions of the retina, by the end stages of the disease, there is severe neuronal loss, including the entire outer retina and gliosis throughout the eye (Goebel, 1992; Hofman et al., 1999; Bensaoula et al., 2000). These degenerating photoreceptors do not accumulate autofluorescent storage material, indicating that, at least in this class of cells, ceroid accumulation is not a primary cause of cell death (Bensaoula et al., 2000). Using an antibody specific to CLN3, Katz and colleagues showed immunopositive Muller cells and inner retinal neurons. However, little labeling was observed in photoreceptor cells, indicating that the viability of these cells is not directly regulated by the expression of CLN3 (Katz et al., 1997). Clinical evidence suggests that degeneration of visual processing extends outside of the retina, with fundoscopy of Batten patients revealing atrophy of the retinal vasculature and the optic nerve head (Spalton et al., 1980). Careful evaluation of the cellular basis of this visual deterioration has only been possible at autopsy, thus not allowing the determination if the retina is the primary site of insult to the visual system or if this site of insult lies outside of the retina. Therefore, animal models of the NCL disease will provide a better system for a careful evaluation of the time course of these changes.

In this study, we utilize a mouse model of Batten disease, the *Cln3* knockout (*Cln3*$^{-/-}$) mouse (Mitchison et al., 1999), to explore the pathology of visual deficits resulting from a loss of *Cln3*. Previous studies on *Cln3*$^{-/-}$ mice have shown limited changes within the retina (Seigel et al., 2002). These subtle changes included increased autofluorescence in the retinal ganglion cell layer and decreased nerve fiber density within the retina, although no changes have been reported prior to 12 months of age (Seigel et al., 2002). *Cln3*$^{-/-}$ mice also had electroretinograms (ERGs) that appear completely normal (Seigel et al., 2002). Taken together, these data suggest only limited dysfunction, if any, within the retina of *Cln3*$^{-/-}$ mice. Interestingly, examination of the optic nerve revealed more profound deficits, including a reduction in optic nerve myelination as well as loss of RGC axons and overall axonal atrophy (Sappington et al., 2003), suggesting that pathological events maybe be occurring outside of the retina that leads to visual deterioration.

Focusing on this potential for changes outside of the retina, we demonstrate that degeneration within retino-recipient nuclei combined with retrograde deterioration of the optic nerve precedes retinal cell loss, confirming that the effect of mutations in *Cln3* on retinal cells is only secondary. In investigating whether the loss of *Cln3* leads to a functional impairment within visual processing, we uncovered a physiological decrease in the

NIH-PA Author Manuscript

NIH-PA Author Manuscript

NIH-PA Author Manuscript

conduction velocity of signals propagated from the RGCs to central visual processing regions via the optic nerve. Stereological analysis of these RGC afferent nuclei in *Cln3*$^{-/-}$ mice revealed selective cell loss within the dorsal lateral geniculate nucleus (LGNd). Recent studies on elucidating the function of CLN3 have implicated this protein in intracellular amino acid movement and protein trafficking (Kim et al., 2003; Fossale et al., 2004; Luiro et al., 2004; Weimer et al., 2005). Therefore, we examined whether there was impaired axonal transport of amino acids in the *Cln3*$^{-/-}$ mice and observed a decrease in the movement of [^{3}H]-proline from the retina to the LGN. This study provides the first evidence for early pathological changes within the thalamus and optic nerve which contribute to the degeneration of visual processing in *Cln3*$^{-/-}$ mice and provides valuable insights into understanding the pathogenesis of Batten disease.

Materials and methods

Animal husbandry

129/SvJ and homozygous *Cln3* knockout (*Cln3*$^{-/-}$) mice on a 129/SvJ background were used (Mitchison et al., 1999). All animals were age- and sex-matched and housed under identical conditions. All procedures were carried out in accordance with NIH guidelines and the University of Rochester Animal Care and Use Committee Guidelines.

Processing of retina tissue

Eyes were removed from the mice at postnatal day 0 (P0), 3 months, or 1 year and fixed in 4% paraformaldehyde/0.2 M phosphate buffer (PFA) for 3 h at room temperature. The lens of the eyes were removed, and samples were dehydrated in graded ethanol, cleared in xylenes, and embedded in paraffin via standard protocols. Eyes were sectioned on a paraffin microtome at a thickness of 6 μm, mounted on glass slides, air dried, and stained with Hematoxylin and Eosin via a routine protocol.

Optic nerve immunocytochemistry and electrophysiology

Mice were sacrificed by cervical dislocation and optic nerves dissected followed by fixation in 2% PFA for 30 min at room temperature. Nerves were then sunk successively in 20% and 30% sucrose in 0.1 PB, frozen in O.C.T., sectioned at 10 μm, mounted on gelatin-coated coverslips, and dried. Nerves were permeabilized in a mixture of 0.1 M PB, 0.3% Triton X-100, and 10% goat serum (PBTGS). Cryosections were incubated overnight at 4°C in primary antibodies (polyclonal anti-$Na_V1.6$, a gift of Dr. James S. Trimmer and monoclonal Anti-Ankyrin G antibody, Oncogene, Cambridge, MA) and then washed three times. Goat anti-rabbit Alexa 488 and goat anti-mouse Alexa 546 secondary antibodies (Molecular Probes) were then applied for 1 h at room temperature. All slides were examined with a Nikon Microphot fluorescence microscope fitted with a Hamamatsu C4742-95 cooled CCD camera controlled by Image-Pro (Media Cybernetics).

Details of the electrophysiology technique have been published previously (Rasband et al., 1999; Vabnick et al., 1999). Briefly, compound action potentials were measured by drawing each end of a nerve into a suction electrode, using one side for stimulation and the other for recording. Nerves were bathed in oxygenated Locke's solution, containing (mM): NaCl 154, KCl 5.6, $CaCl_2$ 2, D-glucose 5, and HEPES 10, pH 7.4. Sweeps were collected and analyzed.

Histological processing and Nissl staining

For histological analyses, 6-month-old homozygous *Cln3*$^{-/-}$ and age- and sex-matched 129/SvJ controls (n = 3 animal per genotype) were fixed by transcardial perfusion. Mice were first deeply anaesthetized with sodium pentobarbital (100 mg/kg i.p.) and transcardially

NIH-PA Author Manuscript

NIH-PA Author Manuscript

NIH-PA Author Manuscript

perfused with vascular rinse (0.8% NaCl in 100 mM NaH PO_4) followed by PFA. Brains were removed and post-fixed overnight followed by cryoprotection at 4°C in successive 24 h changes of 20% and 30% sucrose in 0.1 PB. Brains were sectioned into serial 40 μm frozen coronal sections and stored at −80°C in cryoprotectant solution (TBS/30% ethylene glycol/15% sucrose/0.05% sodium azide). To provide direct visualization of neuronal morphology, every third section through the CNS was stained with the Nissl dye cresyl violet. Sections were mounted onto microscope slides, air-dried overnight, and incubated for 45 min at 60°C in 0.05% Cresyl Fast Violet and 0.05% acetic acid (VWR), rinsed in distilled water, and differentiated through a graded series of alcohols before clearing in xylene (VWR) and coverslipped with DPX (VWR). These Nissl-stained sections were subsequently used for stereological analysis of regional volume, and neuron survival, as described previously (Bible et al., 2004; Pontikis et al., 2004).

Measurements of regional volume, neuronal number, and neuronal volume

Unbiased Cavalieri estimates of the volume of the cortex, hippocampus, striatum, thalamus, hypothalamus, and cerebellum were made from each animal, as described previously (Bible et al., 2004; Pontikis et al., 2004), with no prior knowledge of genotype. Regional volumes were expressed in μm^3 and the mean volume of each region calculated for control and homozygous *Cln3*$^{-/-}$ mice. To examine neuronal survival and volume within individual nuclei, we used StereoInvestigator software (MicroBrightField, Inc.) to obtain unbiased optical fractionator estimates from Nissl-stained sections of the total number of neurons in dorsal nucleus of the lateral geniculate nucleus, together with nucleator estimates of neuronal volume in this region. These measures were performed exactly as described previously (Bible et al., 2004; Pontikis et al., 2005), with a random starting section chosen followed by every sixth Nissl-stained section thereafter. The boundaries of LGNd were defined by reference to landmarks in a brain atlas (Paxinos and Franklin, 2001). Only neurons with a clearly identifiable nucleus were sampled, and all counts were carried out using a 100× oil objective (NA 1.4).

Intraocular injection of ^{3}H-proline

Animals were anesthetized with an intraperitoneal injection of 0.250 mg/g Avertin. Once sedated, 129/SvJ and *Cln3*$^{-/-}$ mice received an intravitreal injection of 3 μL of L-[2,3,4,5 ^{3}H] proline (Amersham Biosciences, Pittsburgh, PA, concentration 1.0 mCi/mL) in a sterile aqueous solution containing 2% ethanol delivered using a Hamilton syringe and 33 GA needle. Vital signs were monitored on all animals during the procedure and, when needed, animals were supplemented with 0.05 mg/g Avertin. Following injections, animals were allowed to recover for either 4, 8, or 16 h. Animals were then sacrificed, and the retina, optic nerve, and LGN dissected out. The optic nerve was processed into approximately 1.0 mm pieces and placed into Ecoscint H scintillation fluid (National Diagnostics) and read on a scintillation counter for 5 min for ^{3}H content. LGN and retina samples were subsequently homogenized in 450 μL of buffer (0.5 mM DTT, 50 mM sodium phosphate buffer, pH 7.5) using a mechanical tissue homogenizer. Three replicates of 100 μL each were then added to 5 mL Ecoscint H for reading on the scintillation counter. To determine whether any radiation was incorporated into newly synthesized proteins, a TCA precipitation was done using standard techniques (1999). The remaining 100 μL of LGN protein samples was then mixed with 500 μL of 5% TCA. Samples were incubated on ice for 1 h and then filtered through a Millipore vacuum filtration system onto GF/C microfiber filters (Whatman, Maidstone, UK). Samples were washed twice with 5 mL of 5% TCA followed by 3 washes with 5 mL 100% ethanol and allowed to air dry and read on a scintillation counter. All scintillation counts are reported as disintegrations per minute (DPM).

NIH-PA Author Manuscript

NIH-PA Author Manuscript

NIH-PA Author Manuscript

Statistical analysis

For physiological experiments, differences in conduction velocity were calculated by determining the area under the trace recording and performing Mann–Whitney *t* test. Significance was determined as $P \leq 0.05$. For all stereological analyses, significance of differences between genotypes was assessed using a one-way ANOVA (SPSS 11.5 software, SPSS Inc.), with statistical significance considered at $P \leq 0.05$. The mean coefficient of error (CE) for all individual optical fractionator and nucleator estimates was calculated according to the method of Gundersen and Jensen (1987) and was less than 0.08 in all analyses (Gundersen and Jensen, 1987). For comparisons of proline transport to the LGN, comparisons of DPMs were performed using Student's *t* test, with statistical significance considered at $P \leq 0.05$, $n = 4$.

Results

Preservation retina in Cln3$^{-/-}$ mice

The first clinical pathology associated with most forms of the NCL diseases is visual deterioration. Children with JNCL show profound loss of cells within the retina by the mid stages of their disease progression, suggesting that these visual deficits begin with degeneration of this structure (Bensaoula et al., 2000). To explore whether similar retinal deterioration is seen in an animal model as in JNCL patients, we have made use of the *Cln3* knockout (*Cln3*$^{-/-}$) mouse (Mitchison et al., 1999). Nissl-stained sections of the retina of *Cln3*$^{-/-}$ mice show no apparent difference from age-matched, sex-matched control mice up to 12 months of age (Fig. 1). Higher magnification revealed that the overall thickness of each cellular layer in the *Cln3*$^{-/-}$ mice retinas was comparable to that of the control mice and the laminar structure of the retina was maintained as late as 12 months of age, indicative of minimal cell loss by this time point. These findings suggest that visual deficits within the *Cln3*$^{-/-}$, and possibly JNCL children, are not the direct result of deterioration in the retina but might be the result of cellular changes in other regions of higher visual processing.

Optic nerve

Processing of vision information from the retina to central regions requires proper propagation of information down the optic nerve where information is distributed to the superior colliculus (SC), suprachiasmatic nucleus (SCN), or the lateral geniculate nucleus (LGN). Recent evidence has shown that the axonal density as well as the myelination of the optic nerve in *Cln3*$^{-/-}$ mice is substantially decreased (Sappington et al., 2003). We therefore sought to use *Cln3*$^{-/-}$ mice to establish structural and functional changes occurring within the optic nerve which might contribute to deficits in visual processing.

To address this issue, we examined nerve propagation in wild-type and mutant *Cln3* mouse optic nerves by collecting compound action potentials (CAPs) recordings. We in turn recorded conduction velocities from 6-month-old optic nerves using suction electrodes. CAP measurements represent the sum of action potentials from a population of axons. While the general shape of the CAPs did not differ between wild-type and null mutant animals (Fig. 2A), the average conduction velocity of the wild-type optic nerves was 22% faster than that of null mutants (Fig. 2B) ($n = 12$; 129/SvJ = 2.7 m/s; *Cln3*$^{-/-}$ = 2.1 m/s; Mann–Whitney *U* test, $P = 0.01$).

CLN3 has been reported to interact with Hook1, a cytosolic endosome-associated protein which functions to stabilize organelles in the endocytic, late endocytic, and lysosomal pathways (Kramer and Phistry, 1996; Luiro et al., 2004). We have subsequently shown that Hook1 protein interacts with Ankyrin G, a spectrin-binding protein that couples the cytoskeleton to the cytoplasmic domains of integral membrane proteins (Bennett, 1992;

NIH-PA Author Manuscript

NIH-PA Author Manuscript

NIH-PA Author Manuscript

Wood and Slater, 1998). Ankyrin G is believed to anchor voltage-gated sodium channels at the axon initial segments, the Nodes of Ranvier, and the post-synaptic folds of the neuromuscular junction (Bennett, 1992; Kordeli et al., 1995; Wood and Slater, 1998; Jenkins and Bennett, 2001). Therefore, we investigated whether there were changes in the morphology of the optic nerve that accounted for the decrease in conduction velocity in mutant mice. $Na_v1.6$ is a Na^+ channel subtype that is found clustered along with Ankyrin G at Nodes of Ranvier in the nervous system and is a good marker for confirming nodal location in axons (Rasband et al., 2001, 2003). Double labeling *Cln3*$^{-/-}$ optic nerves for $Na_v1.6$ and Ankyrin G showed no visible difference in nodal shape or intensity (Fig. 3). These findings suggest that, morphologically, the axons of the retinal ganglion cells within the optic nerve remain intact while there is a decrease in conduction velocity between the retina and more central visual processing regions.

Cell loss in retinal projection regions

Communication between the retina and projection regions within the brain allows for proper segregation of vision information and relaying of this information on to higher cortical processing regions. Deterioration in any of these regions, which include the SC, SCN, and the dorsal LGN (LGNd), could adversely impact visual processing and lead to the degeneration of cells either retrograde (retina) or anterograde (LGNd or primary visual cortex [V1]) to the site of insult. To determine whether these regions were affected in the *Cln3*$^{-/-}$ mice, we examined the anatomical organization of the retinal projection regions. Low power micrographs of the SC, LGN, and SCN show no obvious structural changes (Fig. 4). Next, we determined whether there were any changes in Cavalieri estimates of volume of these regions in 6-month-old *Cln3*$^{-/-}$ mice compared to wild-type controls. These data revealed no decrease in the overall volume of any of the regions examined (Fig. 5).

Although the overall volume of the LGNd was maintained, closer examination revealed an apparent decrease in the number of large projection neurons within the *Cln3*$^{-/-}$ mice (Fig. 4). Therefore, to quantify cell loss within this nucleus, we performed unbiased optical fractionator counts of the large projection neurons within the LGNd as well as counts of the small neuronal cells within the region, which includes the small inhibitory interneurons, endothelial cells, and glial. We noted a significant decrease of nearly 25% in the number of the large projection neurons in the LGNd of the *Cln3*$^{-/-}$ mice, which receive input from the retina and relay it to V1 (Fig. 6). Of the remaining large neurons, there was no change in individual neuron volume, indicating that the remaining cells are not atrophied and appear relatively healthy (data not shown). There was no change in the number of small neuronal cells in the LGNd, suggesting that remaining neurons and support cells are able to maintain the regional volume (Fig. 6).

Deterioration in the visual pathway results in interrupted transport between the retina and LGN

Cellular insult within the thalamus could trigger the previously described increases in astrocytic and microglial activation (Pontikis et al., 2004). Although the exact function of CLN3 remains unclear, recent studies have suggested a role of this protein in the intracellular transport of amino acids and protein trafficking (Kim et al., 2003; Fossale et al., 2004). Proper protein trafficking and communication between the retina and central visual processing regions are imperative for maintenance of cells within both regions. Therefore, we examined whether there was a disruption in fast axonal transport of amino acids in the optic nerve. When injected into the vitreous humor, [^{3}H]-proline will be taken up by the adjacent RGCs and transported down the length of their axons to the SC, LGN, or SCN. Although some amount of proline will be synthesized into new proteins, the rate of axonal transport is far faster than synthesis of new proteins, allowing for the direct measure of fast

NIH-PA Author Manuscript

NIH-PA Author Manuscript

NIH-PA Author Manuscript

axonal transport. Animals were anesthetized, and [^{3}H]-proline was injected intraocularly in an amount in excess to what can be transported in a 16 h period. Following a recovery period of 4 h, when the proline would primarily be in the retina and proximal optic nerve; 8 h, when the proline would be primarily in the optic nerve; or 16 h, when the amino acid would have had sufficient time to reach the LGN, animals were sacrificed and tissue harvested. First, optic nerves were sectioned into 1 mm sections, and the amount of [^{3}H]-proline within each sample was measured. Plotting of DPM counts per segment of optic nerve revealed a substantial decrease in the amount of [^{3}H]-proline transported within the optic nerve at 16 h post-injection (Fig. 7C). At 4 h post-injection, a minimal amount of the [^{3}H]-proline has entered the optic nerve, with the highest levels of radiation present in the initial segments (Fig. 7A). By 8 h, the highest levels of [^{3}H]-proline were present in the optic nerve as the amino acid progressed towards the optic chiasm and LGN (Fig. 7B). By 16 h post-injection, when the [^{3}H]-proline has traveled down the optic nerve and into the LGN, there was an obvious difference in the levels of amino acid in the *Cln3*$^{-/-}$ optic nerve (Fig. 7B).

To further explore differences in amino acid transport within the optic nerve, samples of LGN were homogenized, and the amount of radiation within each sample was measured. Although no difference was seen at the earlier time points, by 16 h post-injection, there was a significant decrease in the amount of [^{3}H]-proline within the LGN of *Cln3*$^{-/-}$ mice compared to controls (Fig. 7D). Samples from each LGN were subsequently processed for TCA precipitation to determine whether there were differences in the amount of [^{3}H]-proline incorporated into newly synthesized proteins, but no differences were evident (data not shown). Therefore, the difference in [^{3}H]-proline detected in the LGN in the *Cln3*$^{-/-}$ mice must be the result of a decrease in the rate of transport of the amino acid from the retina.

Discussion

Deterioration of vision is typically the first clinical sign to manifest in children with Batten disease. It has been speculated that the cells of the retina have a selective vulnerability to mutations in *CLN3*. In the current study, we employ a mouse model of Batten disease, the *Cln3* knockout (*Cln3*$^{-/-}$) mouse, to explore the pathogenesis of visual deterioration associated to alterations in *Cln3* levels. Previous studies on deterioration of the retina in the *Cln3*$^{-/-}$ mouse have shown limited cell loss (Seigel et al., 2002). Herein, we confirm this preservation of retinal structure, well after time points when pathology in other CNS structures have been reported (Mitchison et al., 1999; Pontikis et al., 2004), suggesting that degeneration within the retina is not the primary site of insult. Interestingly, the preservation of the retina appears to be unique to the *Cln3*$^{-/-}$ mouse as loss of retina cells is much more obvious in other NCL animal models. For instance, the *m*otor *n*euron *d*egeneration (*mnd*) mutation, resulting from a naturally occurring mutation in *Cln8*, has cell loss in the outer nuclear layer by 5 weeks and thinning of the peripheral retina by 2 months. By 6 months, the entire retina has thinned, and the animal is completely blind (Chang et al., 1994). Similarly, the *n*euronal *c*eroid *l*ipo*f*uscinosis (*nclf*) mouse, resulting from a mutation in *Cln6*, although more protracted than the *mnd* mouse, also displays retinal degeneration with atrophy of with cell loss in the outer nuclear layer evident by 16 weeks, within the periphery by 6 months, and through the entire retina by 9 months (Chang et al., 2002). In human JNCL patients, one of the primary sites of insult within the retina is the retinal pigmented epithelium (RPE) (Bensaoula et al., 2000). Although the retinal micrographs presented here lack most of the RPE, preservations of all other layers within the retina would support the idea that the cells of the RPE are also preserved as loss of cells within this region could directly affect the survival of cells throughout the retina.

NIH-PA Author Manuscript

NIH-PA Author Manuscript

NIH-PA Author Manuscript

In the current study, we posit that deficits of optic nerve conduction and degenerative loss of cells within central visual processing regions precipitate the visual deterioration associated with mutation in *Cln3*. Although the ultrastructure of the optic nerve itself appears intact, previous studies have described a decrease in myelination and axon density, which could contribute to the decrease in nerve conduction (Sappington et al., 2003). In examining cell numbers within the superior colliculus, lateral geniculate nucleus, and suprachiasmatic nucleus, we observed a selective loss of the large projection neurons within the dorsal portion of the lateral geniculate (LGNd). Cellular insult within LGNd has been noted in other neurodegenerative diseases that have visual deterioration as one of the early hallmarks of the disease, including Creutzfeldt–Jakob disease, Huntington's disease, and Alzheimer's disease (Brown et al., 1986; de la Monte et al., 1988; Wong-Riley et al., 1997; Berman et al., 1998).

In the rodent, virtually all of the retinal ganglion cells project directly to the superior colliculus with a subpopulations of these projections sending collaterals to the LGNd (Perry et al., 1983). Within the human, the LGNd is the primary efferent target for the retinal projection. This difference alone could explain why degeneration of the retina is much more severe in JNCL patients than in $Cln3^{-/-}$ mice as loss of cells within the LGN would have a more pronounced effect on visual processing within the human than seen in $Cln3^{-/-}$ mice. Although we have not explored all efferent LGNd targets, it is possible that cell death in this nucleus leads to retrograde insults in other regions of the brain. Of interest, we did examine the SCN for volumetric difference. In addition to receiving inputs from the retina, the SCN also receives projections from the LGN. One study has shown that bilateral ablation of the LGN was insufficient to cause cellular changes within the SCN but that concomitant axotomy of afferent fibers from the retina was required to elicit cellular alterations (Ueda et al., 1996).

These findings support our thesis that neurons within the thalamus are selectively vulnerable to insult in the $Cln3^{-/-}$ mice and may be the principal determinant of dysfunctional visual processing. In the absence of examination of the timing of cell death of all efferent and afferent LGNd connections, we cannot exclude that cellular damage in a site retrograde to this nucleus may also be contributory. In the current study, we employed 6-month-old mice, a time point in mid-adulthood during which pathological event has been described in other brain regions. Once information is processed though the LGNd, it is relayed to the primary visual cortex, making it possible that cellular changes within V1 might precede or occur concomitant with LGNd cell loss. Ablation of cells within the primary visual cortex (V1) has been shown to lead to the retrograde degeneration of neurons in the LGNd (Lashley, 1941), therefore, such a loss of cells within the cerebral cortex might trigger cell loss in the LGNd. Whereas cortical ablation of V1 leads to degeneration of the large projection neurons within LGNd, the GABAergic interneurons within this thalamic nucleus are spared cell death (Al-Abdulla and Martin, 2002). Interestingly, the $Cln3^{-/-}$ mice suffer selective loss of the large projection neurons with no loss in this small cell population.

Alternatively, if the LGNd was the primary site of insult, selective cell loss could promote both anterograde secondary cell loss within the primary visual cortex as well as optic nerve atrophy and eventual retrograde loss of retinal ganglion cells. At 6 months of age, there was a near 25% reduction in the number of projection neurons within the LGNd of $Cln3^{-/-}$ mice, while at 11 months of age, electroretinograms remained robust, demonstrating limited retinal dysfunction (Seigel et al., 2002). A similar selective loss of neurons in the LGN has been observed in an experimental model of Neuro-AIDS in which animals had an approximate 25% reduction in the cells of the parvocellular layer of the LGNd. Like the $Cln3^{-/-}$ mice, functional impairment was limited as only a portion of these animals had a detectable change in their visual evoked potentials (Berman et al., 1998). In JNCL patients,

NIH-PA Author Manuscript

NIH-PA Author Manuscript

NIH-PA Author Manuscript

photoreceptors in the peripheral portion of the retina appear to be among the first to manifest degeneration (Bensaoula et al., 2000). Information from the retina is conveyed to the LGN topographically. Therefore, understanding whether there is topographically relevant cell death within the LGNd within corresponding regions may elucidate this pathway of degeneration.

Although the exact function of CLN3 remains unclear, recent studies have suggested a role for this protein in the intracellular transport of amino acids and protein trafficking. Specifically, deletion of the yeast homolog of *CLN3, BTN1,* leads to a disruption in the intracellular transport of basic amino acids (Kim et al., 2003). In mammalian cells, mutations in CLN3 have been implicated in a disruption in protein trafficking (Fossale et al., 2004). This protein trafficking may be mediated through a recently reported interaction of CLN3 with Hook1, a member of a family of microtubule-binding proteins implicated in the localization of distinct types of cellular organelles (Walenta et al., 2001; Luiro et al., 2004). It has been shown that loss of *Cln3* leads to substantial increase in the levels of Hook1 (Weimer et al., 2005). Proper protein trafficking and communication between the retina and central visual processing regions are imperative for maintenance of cells within both regions. Axonal transport is essential for proper neuronal function. In addition to the anterograde supply of nutrients and proteins to the nerve terminal, retrograde signaling provides, among other valuable information, trophic information to the cell body. In examining whether disruption in this flow of transported material occurs within the optic nerve following loss of *Cln3*, we demonstrated that, by 16 h post-injection, there was a substantial decrease in the amount of free [^{3}H]-proline transported to the LGN. One cannot rule out the possibility that there is decreased uptake of proline into the retina, particularly at the earlier time point, which contributes to the diminished amounts of radiolabeled amino acid being transported throughout the optic nerve. The lack of differences seen between control and null mice in the amount of proline incorporated into newly synthesized proteins within the retina would suggest that similar amounts of the amino acid are being uptaken by the RGCs. The resulting decrease in transport within the optic nerve could be multifactorial and no mechanism exclusive of others. First, if CLN3 is required for protein trafficking, loss of this protein within the retinal ganglion cells could lead to a decrease in axonal transport. Secondly, if loss of cells within the LGNd or the primary visual cortex is the primary site of insult within the visual pathway, loss of cells within these regions could lead to degeneration of the optic nerve, leading to decreased axonal transport. Thirdly, optic nerve degeneration could be the primary site of insult with decreased axon number resulting in the impaired axonal transport. Alternatively, one cannot exclude the possibility that aberrant development might affect the axonal growth from the RGC to the LGN, influencing not only protein transport but also the survival and function of cells within both regions. Therefore, further analysis of axonal transport is necessary. Furthermore, by using autoradiography to examine the topographic transport of proline to the LGNd, one could identify which retinal cell populations are highly vulnerable.

In the current study, we have established that, in the setting of limited retinal degeneration, the *Cln3*$^{-/-}$ mouse recapitulates progression of visual deficits observed in JNCL patients. Although pathological examinations of disease progression are not possible in affected children, physiological and neuroimaging studies can determine whether consequent changes occur and whether they precede retinal degeneration. In addition to providing a plausible mechanism to explain the retinal degeneration in JNCL patients, the data described herein illustrate a progressive neurodegenerative disease process with attendant visual deficits likely referable to principal damage to the LGN and/or primary visual cortex rather than the retina.

NIH-PA Author Manuscript

NIH-PA Author Manuscript

NIH-PA Author Manuscript

Acknowledgments

The authors wish to thank Dr. Peter Shrager for the generous use of his microscope, camera, and electrophysiology setup for data collection; Charlie Pontikis for assistance in analysis of stereology data; and Timothy Curran, Andrew Serour, and Sarah Leistman for technical assistance. This work was funded in part by National Institutes of Health (NIH) NS40580 and NS44310 (DAP), NS41930 (JDC), training grant support NIH T32 MH065181 (JMW), a student fellowship from the Batten Disease Support and Research Association (JWB), a De Kiewet fellowship (EK) and the European Commission 6th Framework Research Grant LSHM-CT-2003-503051 (JDC, NAA).

References

Al-Abdulla NA, Martin LJ. Projection neurons and interneurons in the lateral geniculate nucleus undergo distinct forms of degeneration ranging from retrograde and transsynaptic apoptosis to transient atrophy after cortical ablation in rat. Neuroscience. 2002; 115:7–14. [PubMed: 12401317]

Bennett V. Ankyrins. Adaptors between diverse plasma membrane proteins and the cytoplasm. J Biol Chem. 1992; 267:8703–8706. [PubMed: 1533619]

Bensaoula T, Shibuya H, Katz ML, Smith JE, Johnson GS, John SK, Milam AH. Histopathologic and immunocytochemical analysis of the retina and ocular tissues in Batten disease. Ophthalmology. 2000; 107:1746–1753. [PubMed: 10964839]

Berman NE, Raymond LA, Warren KA, Raghavan R, Joag SV, Narayan O, Cheney PD. Fractionator analysis shows loss of neurons in the lateral geniculate nucleus of macaques infected with neurovirulent simian immunodeficiency virus. Neuropathol Appl Neurobiol. 1998; 24:44–52. [PubMed: 9549728]

Bible E, Gupta P, Hofmann SL, Cooper JD. Regional and cellular neuropathology in the palmitoyl protein thioesterase-1 null mutant mouse model of infantile neuronal ceroid lipofuscinosis. Neurobiol Dis. 2004; 16:346–359. [PubMed: 15193291]

Brown P, Cathala F, Castaigne P, Gajdusek DC. Creutzfeldt– Jakob disease: clinical analysis of a consecutive series of 230 neuro-pathologically verified cases. Ann Neurol. 1986; 20:597–602. [PubMed: 3539001]

Chang B, Bronson RT, Hawes NL, Roderick TH, Peng C, Hageman GS, Heckenlively JR. Retinal degeneration in motor neuron degeneration: a mouse model of ceroid lipofuscinosis. Invest Ophthalmol Visual Sci. 1994; 35:1071–1076. [PubMed: 8125718]

Chang B, Hawes NL, Hurd RE, Davisson MT, Nusinowitz S, Heckenlively JR. Retinal degeneration mutants in the mouse. Vision Res. 2002; 42:517–525. [PubMed: 11853768]

Consortium IBD. Isolation of a novel gene underlying Batten disease. Cell. 1995; 82:949–957. [PubMed: 7553855]

de la Monte SM, Vonsattel JP, Richardson EP Jr. Morphometric demonstration of atrophic changes in the cerebral cortex, white matter, and neostriatum in Huntington's disease. J Neuropathol Exp Neurol. 1988; 47:516–525. [PubMed: 2971785]

Fossale E, Wolf P, Espinola JA, Lubicz-Nawrocka T, Teed AM, Gao H, Rigamonti D, Cattaneo E, MacDonald ME, Cotman SL. Membrane trafficking and mitochondrial abnormalities precede subunit c deposition in a cerebellar cell model of juvenile neuronal ceroid lipofuscinosis. BMC Neurosci. 2004; 5:57. [PubMed: 15588329]

Goebel HH. Retina in various animal models of neuronal ceroid-lipofuscinosis. Am J Med Genet. 1992; 42:605–608. [PubMed: 1609843]

Goebel HH, Fix JD, Zeman W. The fine structure of the retina in Jansky–Bielschowsku type of neuronal ceroid lipofuscinosis. Am J Ophthalmol. 1974; 83:70. [PubMed: 835670]

Gundersen HJ, Jensen EB. The efficiency of systematic stereology and its prediction. J Microsc. 1987; 147:229–263. [PubMed: 3430576]

Hofman, I.; Kohlschutter, A.; Santavuori, P.; Gottlob, I.; Goebel, HH.; Lake, BD.; Schutgens, RBH.; Greene, ND.; Leung, K-Y.; Mitchison, HM.; Munroe, PB.; Taschner, PE. The Neuronal Ceroid Lipofuscinses (Batten Disease). IOS Press; Amsterdam, The Netherlands: 1999.

Jenkins SM, Bennett V. Ankyrin-G coordinates assembly of the spectrin-based membrane skeleton, voltage-gated sodium channels, and L1 CAMs at Purkinje neuron initial segments. J Cell Biol. 2001; 155:739–746. [PubMed: 11724816]

NIH-PA Author Manuscript NIH-PA Author Manuscript NIH-PA Author Manuscript

Katz ML, Gao CL, Prabhakaram M, Shibuya H, Liu PC, Johnson GS. Immunochemical localization of the Batten disease (CLN3) protein in retina. Invest Ophthalmol Visual Sci. 1997; 38:2375–2386. [PubMed: 9344361]

Kim Y, Chattopadhyay S, Locke S, Pearce DA. Interaction among Btn1p, Btn2p, and Ist2p reveals potential interplay among the vacuole, amino acid levels, and ion homeostasis in the yeast *Saccharomyces cerevisiae*. Eukaryotic Cell. 2003; 4:281–288. [PubMed: 15701790]

Kordeli E, Lambert S, Bennett V. AnkyrinG. A new ankyrin gene with neural-specific isoforms localized at the axonal initial segment and node of Ranvier. J Biol Chem. 1995; 270:2352–2359. [PubMed: 7836469]

Kramer H, Phistry M. Mutations in the *Drosophila* hook gene inhibit endocytosis of the boss transmembrane ligand into multivesicular bodies. J Cell Biol. 1996; 133:1205–1215. [PubMed: 8682859]

Lashley KS. Thalamocortical connections of the rat brain. J Comp Neurol. 1941; 75:67–121.

Luiro K, Yliannala K, Ahtiainen L, Maunu H, Jarvela I, Kyttala A, Jalanko A. Interconnections of CLN3, Hook1 and Rab proteins link Batten disease to defects in the endocytic pathway. Hum Mol Genet. 2004; 13:3017–3027. [PubMed: 15471887]

Mitchison HM, Bernard DJ, Greene ND, Cooper JD, Junaid MA, Pullarkat RK, de Vos N, Breuning MH, Owens JW, Mobley WC, Gardiner RM, Lake BD, Taschner PE, Nussbaum RL. Targeted disruption of the Cln3 gene provides a mouse model for Batten disease. The Batten Mouse Model Consortium. Neurobiol Dis. 1999; 6:321–334. [PubMed: 10527801]

Paxinos, G.; Franklin, KBJ. The Mouse Brain in Stereological Coordinates. 2nd. Academic Press; San Diego, CA: 2001.

Perry VH, Henderson Z, Linden R. Postnatal changes in retinal ganglion cell and optic axon populations in the pigmented rat. J Comp Neurol. 1983; 219:356–368. [PubMed: 6619343]

Pontikis CC, Cella CV, Parihar N, Lim MJ, Chakrabarti S, Mitchison HM, Mobley WC, Rezaie P, Pearce DA, Cooper JD. Late onset neurodegeneration in the Cln3−/−; mouse model of juvenile neuronal ceroid lipofuscinosis is preceded by low level glial activation. Brain Res. 2004; 1023:231–242. [PubMed: 15374749]

Pontikis CC, Cotman SL, Macdonald ME, Cooper JD. Thalamocortical neuron loss and localized astrocytosis in the Cln3(Del-taex7/8) knock-in mouse model of Batten disease. Neurobiol Dis. 2005:823–836. [PubMed: 16006136]

Rasband MN, Peles E, Trimmer JS, Levinson SR, Lux SE, Shrager P. Dependence of nodal sodium channel clustering on paranodal axoglial contact in the developing CNS. J Neurosci. 1999; 19:7516–7528. [PubMed: 10460258]

Rasband MN, Park EW, Vanderah TW, Lai J, Porreca F, Trimmer JS. Distinct potassium channels on pain-sensing neurons. Proc Natl Acad Sci U S A. 2001; 98:13373–13378. [PubMed: 11698689]

Rasband MN, Kagawa T, Park EW, Ikenaka K, Trimmer JS. Dysregulation of axonal sodium channel isoforms after adult-onset chronic demyelination. J Neurosci Res. 2003; 73:465–470. [PubMed: 12898531]

Sappington RM, Pearce DA, Calkins DJ. Optic nerve degeneration in a murine model of juvenile ceroid lipofuscinosis. Invest Ophthalmol Visual Sci. 2003; 44:3725–3731. [PubMed: 12939285]

Seigel GM, Lotery A, Kummer A, Bernard DJ, Greene ND, Turmaine M, Derksen T, Nussbaum RL, Davidson B, Wagner J, Mitchison HM. Retinal pathology and function in a Cln3 knockout mouse model of juvenile Neuronal Ceroid Lipofuscinosis (batten disease). Mol Cell Neurosci. 2002; 19:515–527. [PubMed: 11988019]

Spalton DJ, Taylor DSI, Sanders MD. Juvenile Batten's disease: an opthalmological assessment of 26 patients. Br J Ophthalmol. 1980; 64:726–732. [PubMed: 7426545]

Ueda S, Aikawa M, Ishizuya-Oka A, Nishimura A, Kawata M. Alteration of serotonergic innervation in the suprachiasmatic nucleus of the rat following removal of input fibers from retina and lateral geniculate nucleus. Neurosci Lett. 1996; 211:97–100. [PubMed: 8830853]

Vabnick I, Trimmer JS, Schwarz TL, Levinson SR, Risal D, Shrager P. Dynamic potassium channel distributions during axonal development prevent aberrant firing patterns. J Neurosci. 1999; 19:747–758. [PubMed: 9880595]

NIH-PA Author Manuscript

NIH-PA Author Manuscript

NIH-PA Author Manuscript

Walenta JH, Didier AJ, Liu X, Kramer H. The Golgi-associated hook3 protein is a member of a novel family of microtubule-binding proteins. J Cell Biol. 2001; 152:923–934. [PubMed: 11238449]

Weimer JM, Chattopadhyay S, Custer AW, Pearce DA. Elevation of Hook1 in a disease model of Batten disease does not affect a novel interaction between Ankyrin G and Hook1. Biochem Biophys Res Commun. 2005; 330:1176–1181. [PubMed: 15823567]

Wong-Riley M, Antuono P, Ho KC, Egan R, Hevner R, Liebl W, Huang Z, Rachel R, Jones J. Cytochrome oxidase in Alzheimer's disease: biochemical, histochemical, and immunohistochemical analyses of the visual and other systems. Vision Res. 1997; 37:3593–3608. [PubMed: 9425533]

Wood SJ, Slater CR. beta-Spectrin is colocalized with both voltage-gated sodium channels and ankyrinG at the adult rat neuromuscular junction. J Cell Biol. 1998; 140:675–684. [PubMed: 9456326]

NIH-PA Author Manuscript

NIH-PA Author Manuscript

NIH-PA Author Manuscript

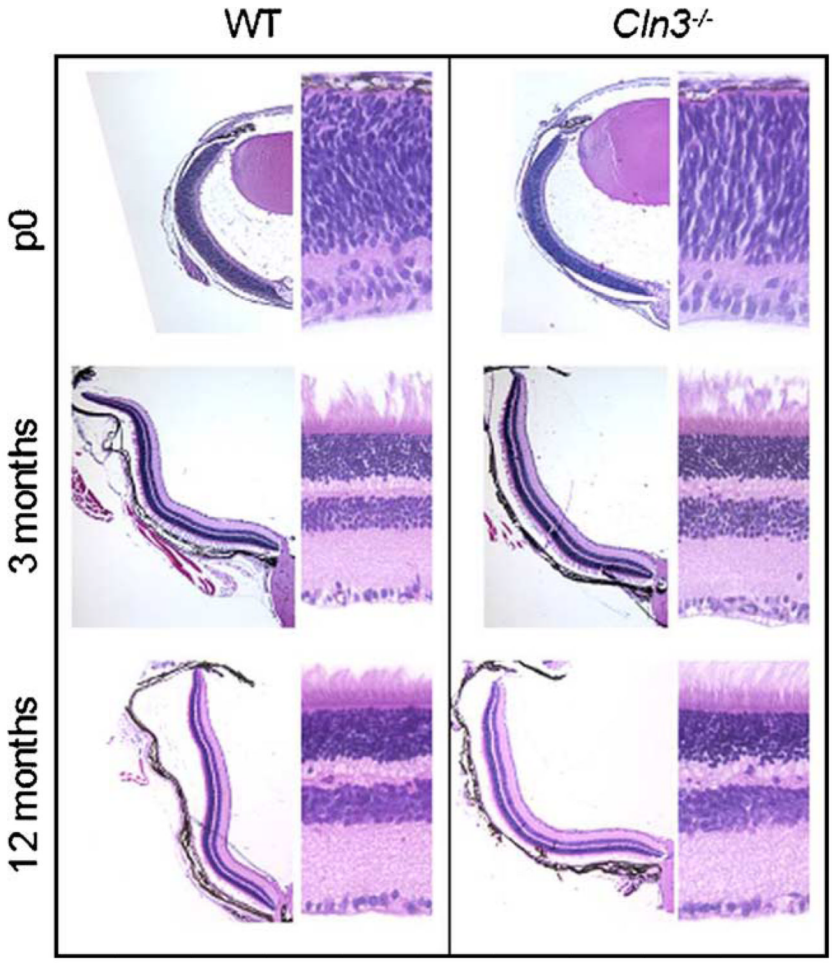

Fig. 1.

No obvious cell loss or structural change in the retina of *Cln3*$^{-/-}$ mice. Comparison of gross morphological changes over time in *Cln3*$^{-/-}$ mice and their respective age-matched wild-type controls. Photographs on the left were taken with a 4× objective and show a section of one retinal hemisphere. Photographs on the right were taken with a 40× objective and show a small subsection of the retina with the ganglion cell layer on the bottom of the image.

NIH-PA Author Manuscript

NIH-PA Author Manuscript

NIH-PA Author Manuscript

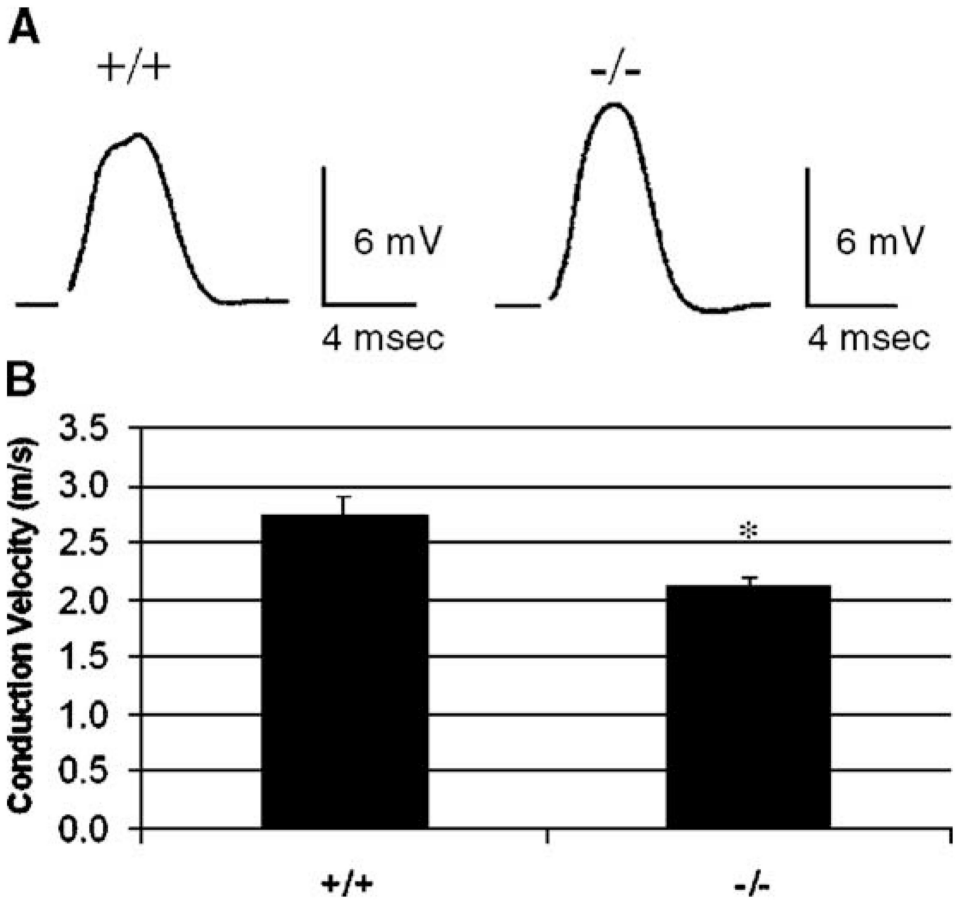

Fig. 2.

Reduction in the conduction velocity of propagated signal in the optic nerve of *Cln3*$^{-/-}$ mice. Sample traces from compound action potentials of 129/SvJ (+/+) and *Cln3*$^{-/-}$ ($^{-/-}$) mouse optic nerves. Sweeps were taken at 25 °C. Scale bars are 6 mV for amplitude and 4 ms for time (A). Average conduction velocities of 129/SvJ and *Cln3*$^{-/-}$ mouse optic nerves (B). The greater conduction velocities of the 129/SvJ optic nerves are statistically significant (*$P < 0.01$ for the two-tailed t test; $P = 0.01$ for the Mann–Whitney U test; mean conduction velocity ± SEM).

NIH-PA Author Manuscript

NIH-PA Author Manuscript

NIH-PA Author Manuscript

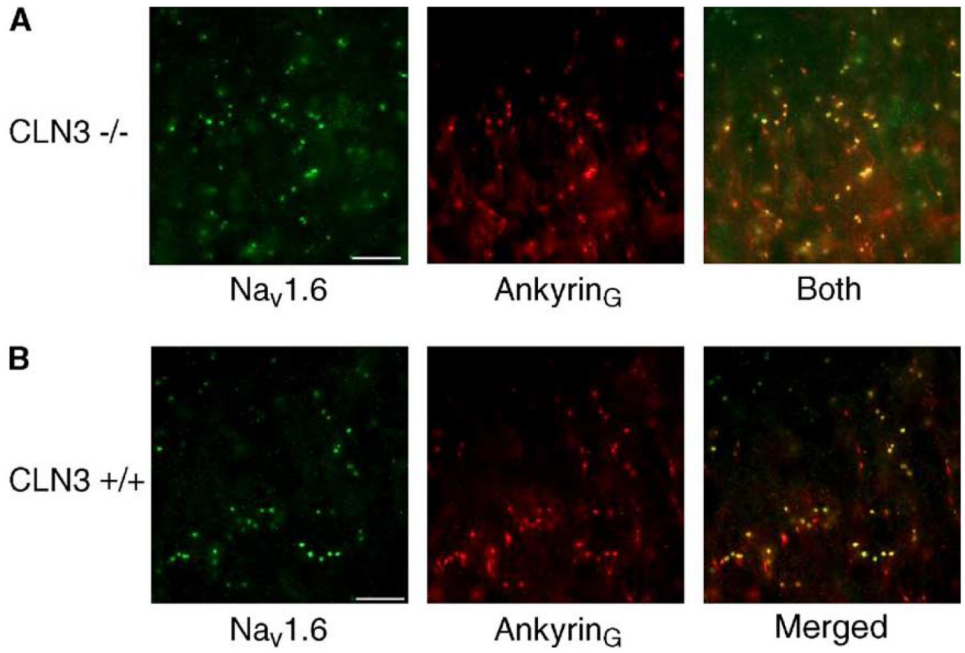

Fig. 3.

Colocalization of $Na_v1.6$ and Ankyrin G in 12-month-old optic nerves of *Cln3*$^{-/-}$ mice. Cryosectioned 12-month-old optic nerves of null mutant and wild-type mice were double-labeled for $Na_v1.6$ and Ankyrin G. Scale bar is 10 μm. *Cln3*$^{-/-}$ mutant optic nerve micrographs of $Na_v1.6$ (green) and Ankyrin G (red), and merged images from a single field of view are shown (A). Overlapping clusters of $Na_v1.6$ and Ankyrin G appear yellow in the merged image. A single representative field of view from $Na_v1.6$ (green) and Ankyrin G (red) labeled wild-type optic nerve (B).

NIH-PA Author Manuscript
NIH-PA Author Manuscript
NIH-PA Author Manuscript

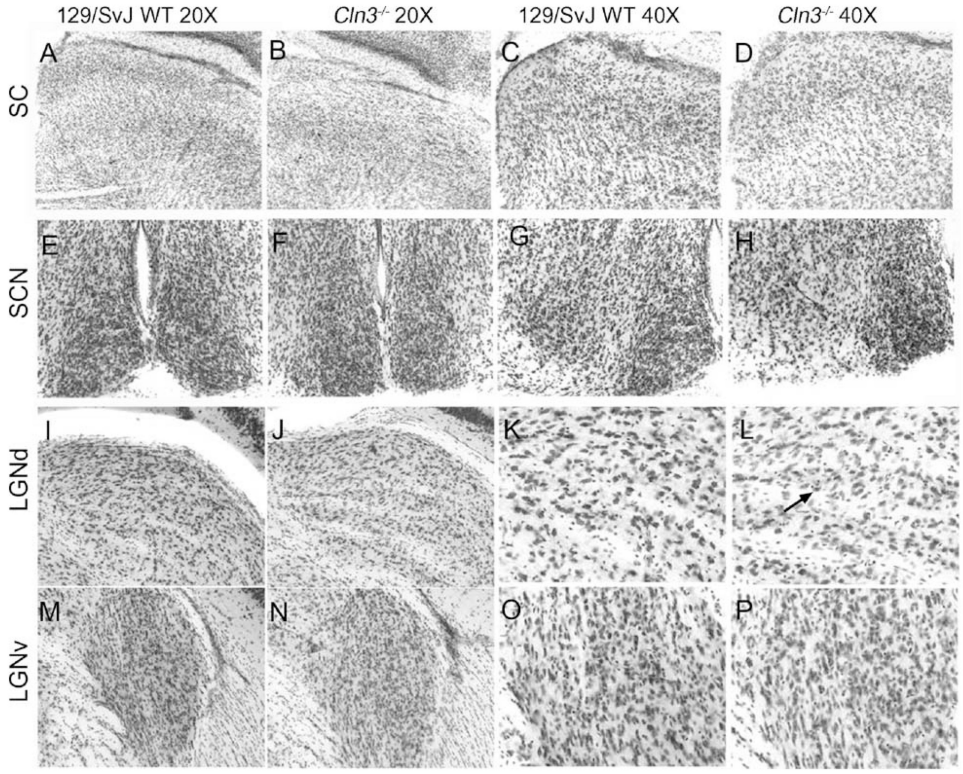

Fig. 4.

Micrograph of the brain regions examined in central visual pathway. Micrographs of Nissl-stained sections were prepared from age and sex-matched 6-month-old 129/SvJ (WT) (A, C, E, G, I, K, M, O) and *Cln3*$^{-/-}$ mice (B, D, F, H, J, L, N, P). Regions represented are the superior colliculus (A–B, 20× and C–D, 40×), suprachiasmatic nucleus (E–F, 20×, G–H, 40×), dorsal lateral geniculate nucleus (I–J, 20× and K–L, 40×), and the ventral lateral geniculate nucleus (M–N, 20× and O–P, 40×). Difference in the cell densities in the dorsal lateral geniculate was apparent, with fewer cells being present in the *Cln3*$^{-/-}$ (L) as compared to the 129/SvJ (K) denoted by the arrow (L).

NIH-PA Author Manuscript

NIH-PA Author Manuscript

NIH-PA Author Manuscript

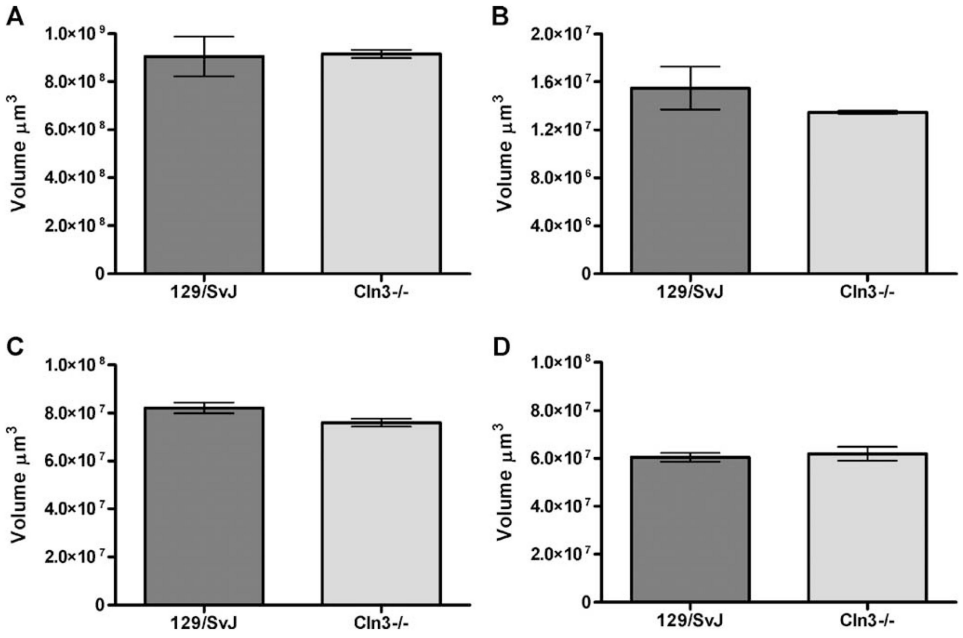

Fig. 5.

Absence of significant regional atrophy in retino-recipient nuclei of the retinal ganglion cells within the visual system of *Cln3*$^{-/-}$ mice. Unbiased Cavalieri estimates of regional volume reveal no significant regional atrophy in *Cln3*$^{-/-}$ vs. 129/SvJ controls (+/+) at 6 months of age. Regions examined included the superior colliculus (A), the suprachiasmatic nucleus (B), the dorsal lateral geniculate nucleus (C), and the ventral lateral geniculate nucleus (D) (mean Cavalieri estimates ± SEM, $n = 3$).

NIH-PA Author Manuscript

NIH-PA Author Manuscript

NIH-PA Author Manuscript

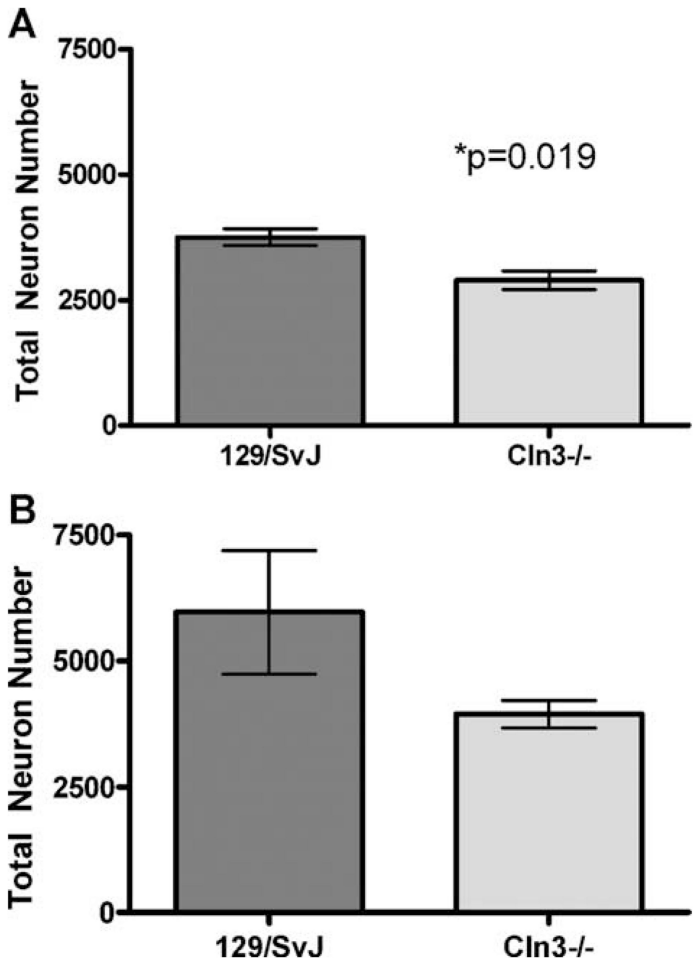

Fig. 6.

Selective loss of large projection neurons in the dorsal lateral geniculate nucleus of 6-month-old 129/SvJ and *Cln3*$^{-/-}$ mice. Optical fractionator estimates of neuronal number revealed the significant loss in the large projection neurons within the dorsal lateral geniculate nucleus of 6-month-old homozygous *Cln3*$^{-/-}$ mice compared with 129/SvJ (WT). These cells receive retinal input from the retinal ganglion cells via the optic nerve (A). In contrast, there was no loss in the number of a mixed population of smaller class B Golgi type II interneurons, glia, and endothelial cells (B) (mean cell fractionator ± SEM, $n = 3$).

NIH-PA Author Manuscript

NIH-PA Author Manuscript

NIH-PA Author Manuscript

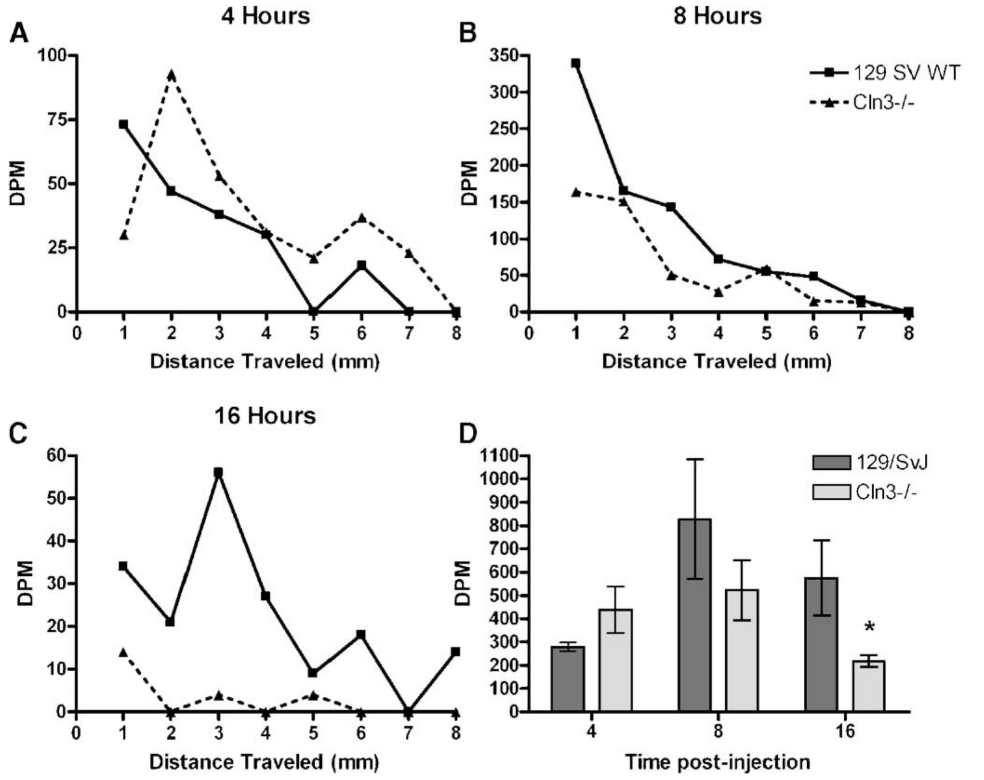

Fig. 7.

Fast axonal transport is decreased in the optic nerve of *Cln3*$^{-/-}$ mice. Animals were anesthetized with an intraperitoneal injection of 0.250 mg/g Avertin. Six-month-old sex- and age-matched 129/SvJ and *Cln3*$^{-/-}$ mice received an intravireal injection of 3 μL of L-[2,3,4,5 ^{3}H] proline and allowed to recover for either 4, 8, or 16 h. Animals were then sacrificed, and the optic nerve and LGN were dissected out. The optic nerve was processed into approximately 1.0 mm pieces and disintegrations per minute (DPM) counts measured by scintillation counter for [^{3}H]-proline content. These readings were plotted as DPM versus distance traveled in millimeters. No differences were observed at 4 or 8 h post-injection, but, by 16 h post-injection, there is an obvious difference in the amount of [^{3}H]-proline being transported in the *Cln3*$^{-/-}$ optic nerve (A–C). LGN were homogenized, and DPM counts read on a scintillation counter. There was a significant decrease in the amount of [^{3}H]-proline transported to the LGN at 16 h post-injection, while no difference was noted at the earlier time point. (D) All scintillation counts are reported as DPM ± SEM, $n = 4$ eyes injected (Student's t test, $^{*}P < 0.05$).